Prototype Imaging Spectrograph for Coronagraphic Exoplanet Studies (PISCES) for WFIRST/AFTA

Qian Gong*[a], Michael McElwain[a] , Bradford Greeley[a], Bryan Grammer[b], Catherine Marx[a], Nargess Memarsadeghi[a], Karl Stapelfeldt[a], George Hilton[c], Jorge Llop Sayson[d], Marshall Perrin[e], Richard Demer[f], Hong Tang[f], Brian Kern[f], Janan Ferdosi[f]

[a]NASA Goddard Space Flight Center, 8800 Greenbelt Road, Greenbelt, MD, USA 20771;
[b]Design Interface, 3451 Gamber Road, Finksberg, MD, USA, 21048;
[c]Newton Engineering, 7100 Chesapeake Road, Suite 202, Hyattsville, MD, USA 20784;
[d]Catholic University of America, 620 Michigan avenue, Washington, DC, USA, 20064;
[e]Space Telescope Science Institute, 3700 San Martin Drive, Baltimore, MD, USA, 21218;
[f]Jet Propulsion Laboratory, 4800 Oak Grove Drive, La Canada Flintridge, CA USA, 91011

ABSTRACT

Prototype Imaging Spectrograph for Coronagraphic Exoplanet Studies (PISCES) is a lenslet array based integral field spectrometer (IFS) designed for high contrast imaging of extrasolar planets. PISCES will be used to advance the technology readiness of the high contrast IFS baselined on the Wide-Field InfraRed Survey Telescope/Astrophysics Focused Telescope Assets (WFIRST/AFTA) coronagraph instrument. PISCES will be integrated into the high contrast imaging testbed (HCIT) at the Jet Propulsion Laboratory and will work with both the Hybrid Lyot Coronagraph (HLC) and the Shaped Pupil Coronagraph (SPC) cofigurations. We discuss why the lenslet array based IFS is selected for PISCES. We present the PISCES optical design, including the similarities and differences of lenslet based IFSs to normal spectrometers, the trade-off between a refractive design and reflective design, as well as the specific function of our pinhole mask on the back surface of the lenslet array to further suppress star light introduced speckles. The optical analysis, alignment plan, and mechanical design of the instrument will be discussed.

Keywords: Integral field spectrometer, lenslet array, coronagraph, pinhole mask

1. INTRODUCTION

Nearly 2000 exoplanets have been discovered so far[1]. However, only a handful of exoplanets have been imaged directly, the vast majority have been detected through indirect methods such as the transit method and the radial-velocity method[2]. WFIRST/AFTA is the first space mission that has an instrument, CoronaGraph Instrument (CGI), dedicated to exoplanets study through direct image method. To meet the intensified interest in the search for extraterrestrial life, the visible spectra of exoplanets are critical to determine planetary habitability. Because the exoplanets in habitable zone are usually very faint, also because we do not know exactly when and where they appear, the IFS becomes an ideal choice to monitor the full high contrast FOV created by coronagraph and record the spectrum at the same time. Besides, the IFS also plays an important role for wavefront sensing of the coronagraph with wide spectral bands.

The PISCES design is driven by the science goals that described in the WFIRST/AFTA science definition team final report[3]. The detailed specification and interface to JPL HCIT will be discussed in Section 2: PISCES overview. In section 3, we'll review the existing IFS options and trade-off, as well as the conclusion to select lenslet array based IFS. In section 4, we present our innovative idea – a combination of optical design, lenslet array and pinhole mask to further increase the contrast and reduce the "speckle" from the stars. In section 5, the detailed optical design and its performance are discussed. Several trade-offs are also discussed, including refractive versus reflective, non-deviation prism versus deviation prism, compound prism versus a single prism. Section 6 presents IFS alignment plan, optical element test, and prototype mechanical design. Section 7 discusses PISCES hardware status and calibration plan. Section 8 discusses prototype test and calibration plan. Finally, the conclusion and path forward from prototype to flight IFS is addressed in Section 9.

*qian.gong-1@nasa.gov; phone 1 301 296-1490; fax 1 301-286-7230

2. PISCES OVERVIEW

As mentioned in the introduction that PISCES system specification is driven by the science goals. As a prototype, PISCES will be tested in HCIT[4] at JPL. HCIT is designed for imaging the coronagraph FOV directly onto a detector array. In order to use HCIT to test IFS, an interface between the HCIT and the IFS is needed. This interface is the relay optics that adjusts the plate scale of the beam to fit the specified FOV onto the designed lenslet array. Figure 1 shows how PISCES is connected to HCIT. In figure 1, the HCIT is on a big optics table. A pick-off mirror and a fold mirror are used to direct the IFS beam above the HCIT. The IFS will be assembled to its own optics bench. It should be mentioned that IFS will be tested under two slightly different configurations. The layout in Figure 1 is for Shaped Pupil Coronagraph (SPC). Another configuration is for Hyper Lyot Coronagraph (HLC). PISCES is compatible to both configurations.

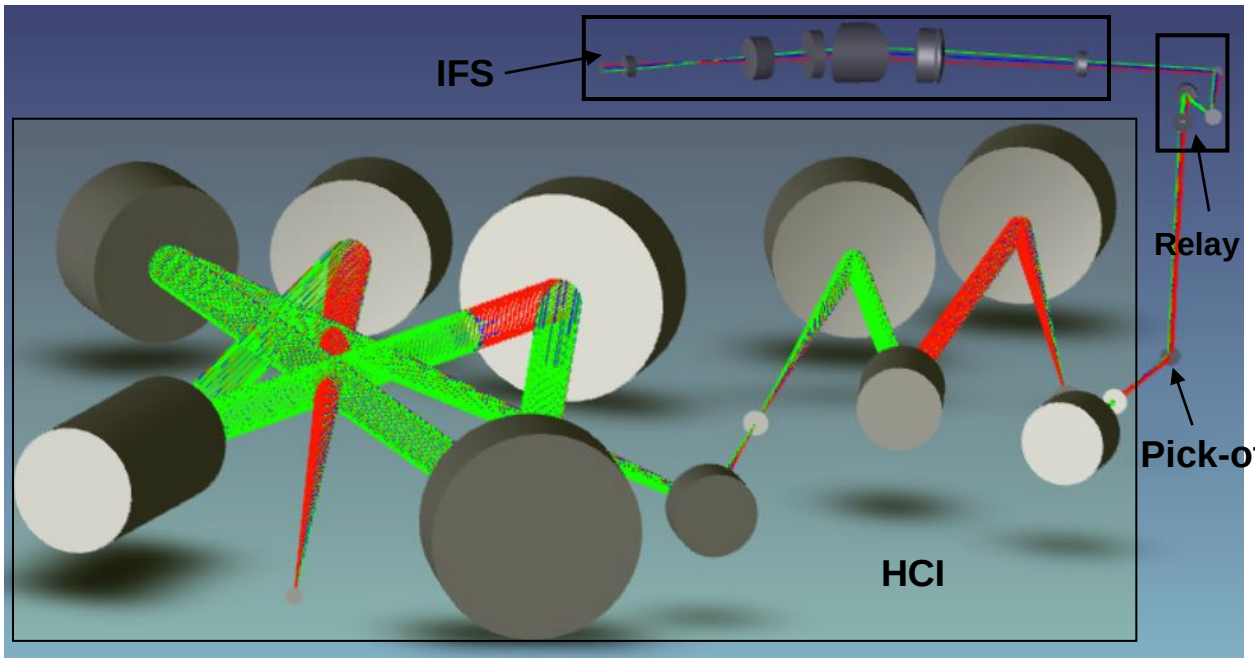

Figure 1. IFS test setup using HCIT.

Under the top science goals, IFS specification is driven by the FOV that the coronagraph clears, the bandwidth $\Delta\lambda$ that meets coronagraph contrast requirement, the total detector size and pixel size, the sampling relative to the Point Spread Function, and the spatial and spectral resolution. Based on the current bandwidth of starlight suppression, the total bandwidth is split into 3 wavelength bands. The specification of the IFS system in summarized in Table 1.

Table 1. Top level specification.

IFS System Specification			
Overall Wavelength Range (nm)	600 - 970		
Spectral Resolution $\lambda/\Delta\lambda$ ($\Delta\lambda$ for 2 pixels)	70		
	Band #1 (18%)	Band #2 (18%)	Band #3 (18%)
Central Wavelength λ_c (nm)	660	770	890
λ_{min} (nm)	600	700	810
λ_{max} (nm)	720	840	970

Sampling at λ_c	3.3	3.85	4.6
FOV (# of λ_c/D)	22.7	19.5	16.9

3. IFS TYPE COMPARISON AND SELECTION

With the specification in place, the first thing is to select IFS type. To date, there are mainly three types of IFS[5] being used: lenslet array, image slicer, and lenslets + fibers. The figure 2 below shows how each IFS works.

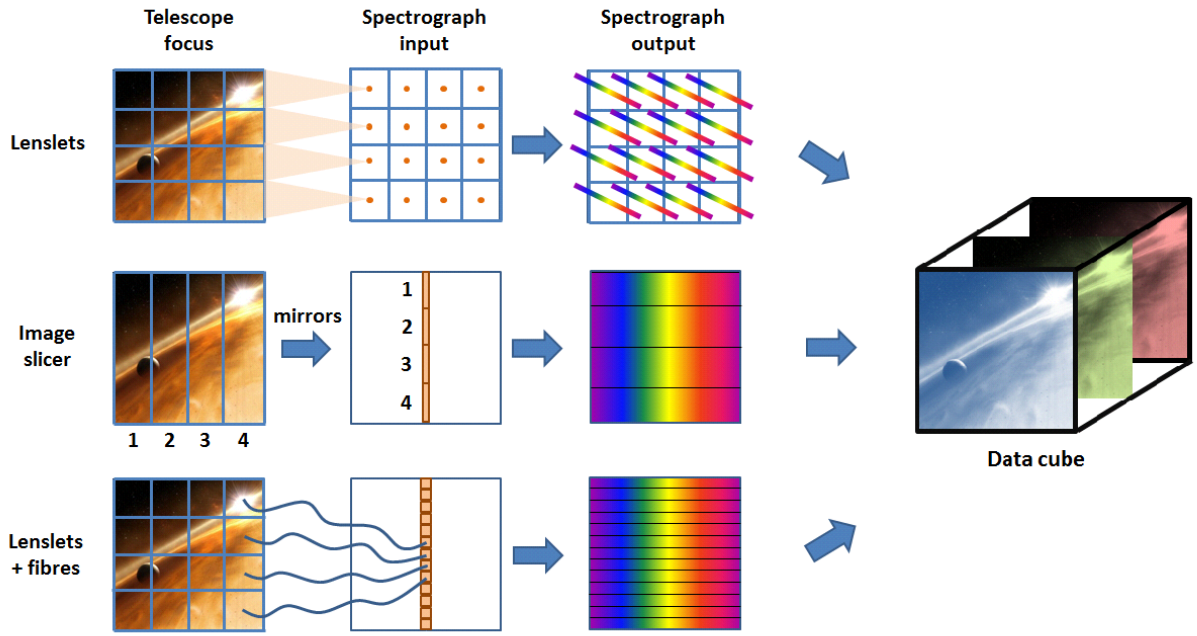

Figure 2. Three main types of IFS: Lenslets, image slicer, and lenslets + fibers.

No matter which type is used, the goal is to obtain 2D image + spectra simultaneously, that is, enough space has to be squeezed out for laying the spectra. Lenslet array achieves it by focusing the light on each lenslet into a tiny spot. Image slicer rearranges multiple image slicers into one line. The lenslets + fibers is the combination of both. It uses lenslets to couple light into the fibers and then rearrange the tips of the fibers to a line. It tried to take the advantage of the simplicity from the lenslets and the high efficiency of detector array usage. However, due to the fiber coupling loss, it is not widely used. Table 2 shows the trade-off of the three types.

Table 2. The comparison of three types IFS.

	Pro	**Con**
Lenslet array	Simplicity High throughput	Lower detector array usage efficiency
Image slicer	Efficient detector array usage	Scattering loss Additional optics is needed to arrange slicers Difficulty to fabricate high number of slices

Lenslets + fiber	Efficient detector array usage	Fiber coupling loss Difficult to align and assemble fibers Fiber material limits wavelength band

Based on the comparison, lenslet array was selected as the IFS for PISCES. The main reason is its high throughput and simplicity. High throughput is critical for any exo-planet instrument because the signal from exo-planet is so weak. Simplicity is always preferred for flight missions due to the lower volume, mass, and cost. The main disadvantage of lenslet array is the low efficiency of detector array usage. However, this is not a problem for PISCES. The small FOV of coronagraph application and low spectral dispersion requirement make it comfortable to layout all spectra onto a 1k x 1k detector array.

For the other two types, the main concern of lenslets + fiber is the throughput loss wfor the light ito couple into the fiber. If the single mode fiber is used, the coupling efficiency is low. If the large core multimode fiber is used, additional optics is needed to de-magnify the fiber tip to match the detector pixel size. The problem of the image slicer is that a complicated optical system is needed to re-arrange a 2D image into a 1D slit. Besides, the state of art image slicer can't provide enough slices to meet the spatial resolution for WFIRST coronagraph.

4. HOW TO USE LENSLET ARRAY TO FURTHER IMPROVE CONTRAST

4.1 Concept of Using Lenslets and Pinhole Mask to Increase Coronagraph Contrast

This section discusses our innovative idea: using the combination of lenslet array and pinhole mask to further suppress the residual star light. In other words, to make the dark hole of the coronagraph even darker[6].

The original idea of using the pinhole mask at the focal plane of the lenslet array is to remove the diffraction lines introduced by the edges of square lenslets. However, combined with a smart optical design, it can also be used to further improve the coronagraph contrast. The basic idea is to design a relay optics that is non-telecentric, that is, the incident angle of the chief ray increases versus the FOV. As we know, the wavefront of any beam at the focus is flat for any diffraction limited beam. The reason is quite straight forward: a beam from converge to diverge at the focus. So the wavefront has to be flat there. It is just like Gaussian beam propagation, at the beam waist, the wavefront is flat. Figure 3 illustrates how the idea works.

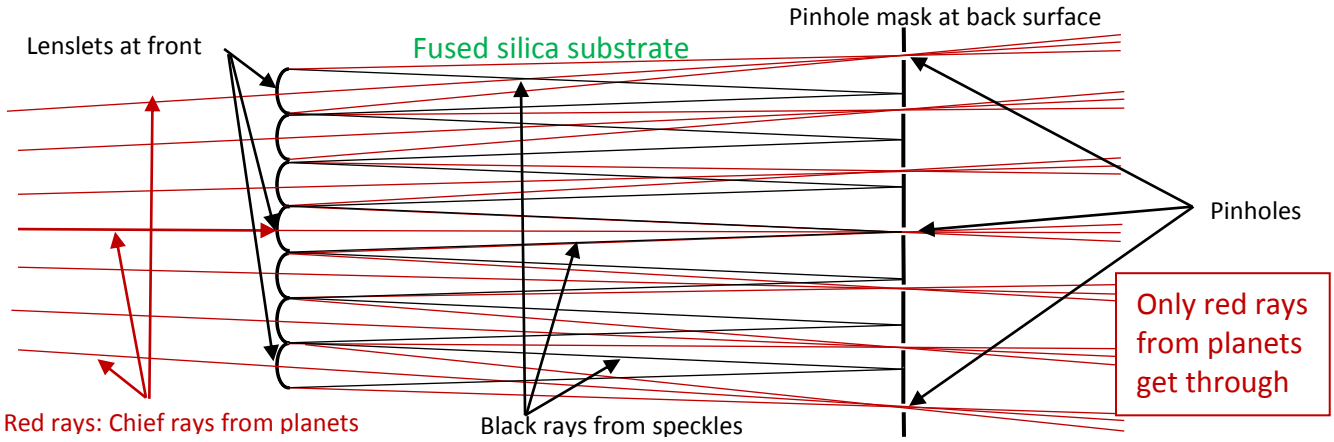

Figure 3. Illustration of using lenslets and pinhole mask to further suppress residual star light.

In figure 3, the incident beam (red rays) on the left is from the relay optics. The beam hits the front surface of a lenslet array in a rectangular grid. The lenslet array is designed in such a way that its focal plane is at the back surface of the lenslet array. The pinhole mask then precisely deposited on the back surface of the lenslet array. The chief ray angle of the incident beam is a function of the FOV. Every lenslet has a different chief ray angle. The position of Point Spread Function (PSF) in the focal plane is determined by the chief ray. Therefore, the pinhole position on the mask has

anoffset from the rectangular grid of the lenslet array. The offset is a function of the chief ray angle. The pinholes follow the chief ray of each lenslet to optimize the throughput of targets: exo-planets. The red rays in Figure 3 are the rays from the targets, the black rays are residual star light called speckles. It is clear from Figure 3 that most of the black rays are blocked by the pinhole mask except the central one. It is obvious, the suppression is also a function of FOV. The rays close to the center have low or no suppression. Fortunately, the FOV for exo-planet exploration starts > 3λ/D.

4.2 PISCES Lenslet Array Design

The lenslet array specification is derived from PISCES top level specification in Table 1. The first parameter that needs to be defined is the size of the lenslet. As mentioned in previous section, the lenslet size is driven by the spectral resolution and detector pixel size. Based on the resolution R = 70 and 18% of wavelength bandwidth, the dispersion length on the detector is 26 pixels. Detector pixel size is 13μm. Considering the 4 pixel separation in dispersion direction and 6 pixel separation in cross dispersion direction between any two adjacent spectra, the lenslet size is calculated as 174 μm x 174 μm[7]. The second parameter is the format of lenslet array, which is determined by the detector size. PISCES detector is a 13.3mm x 13.3mm CCD. So the lenslet format is 76 x 76. The third parameter is the f/# of each lenslet. The f/# determines PSF size. The pixel size of PISCES detector is 13 μm, so f/8 from lenslet side to side is selected. This means that the effective focal length *f* of the lenslet is 1.392mm. Because we want the focal plane on the back surface of the lenslet array, the thickness *t* of the lenslet array is $t = n \cdot f$, where n is the refractive index of lenslet. The material of our lenslet array is fused silica, so the thickness is 2.031mm. Note all the parameters are derived based on the fact that the spectrometer after lenslet array has a unit magnification (1:1).

The lenslet array design is followed by the pinhole mask design. There are two parameters to determine: The diameter and position of pinholes. The diameter is determined by PSF size plus enough tolerance to make sure entire Airy disc passing through. The position of each pinhole, discussed in 4.1, is determined by ray trace. The lenslet array specification is summarized in Table 3.

Table 3. Lenslet array specification.

Lenslet size (μm)	13
Lenslet array format	76 x 76
f/# (square lenslet side to side)	8
Focal length (mm)	1.392
Lenslet array thickness (mm)	2.031
Material	Fused silica
Pinhole diameter (μm)	25
Pinhole pattern	Following the ray trace

4.3 Initial lenslet Test and pinhole Function Demonstration

The initial lenslet array test has been performed. The test up is shown in Figure 4. The test setup is very simple. A HeNe laser at 632.8nm was used as the light source. It was focused by a microscope objective onto a spatial filter. The beam was then collimated and illuminated on the lenslet array. Two lenslet arrays were tested. One with the pinhole mask, and the other one without. A microscope objective was attached to a CCD to provide necessary magnification. The back surface of the lenslet array was imaged onto the CCD.

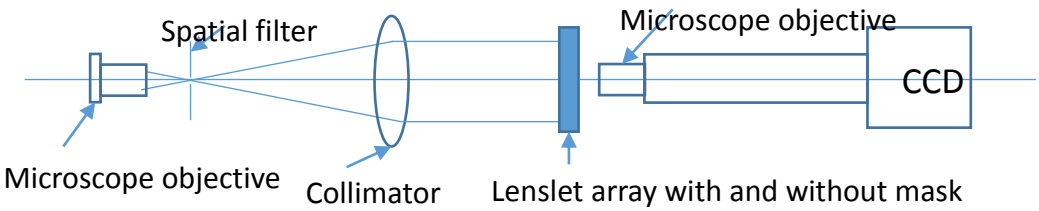

Figure 4. Lenslet array test setup.

The images from the test setup above are shown in Figure 5 (a), (b), and (c).

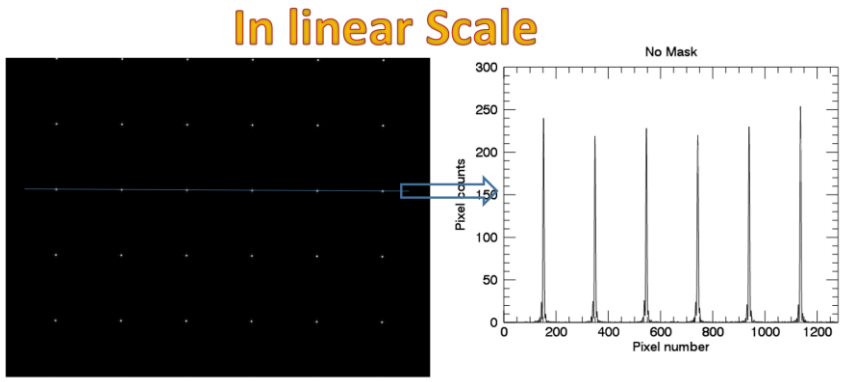

(a)

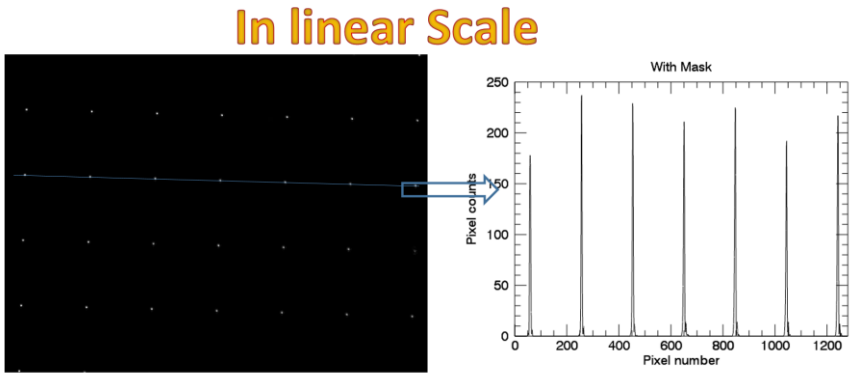

(b)

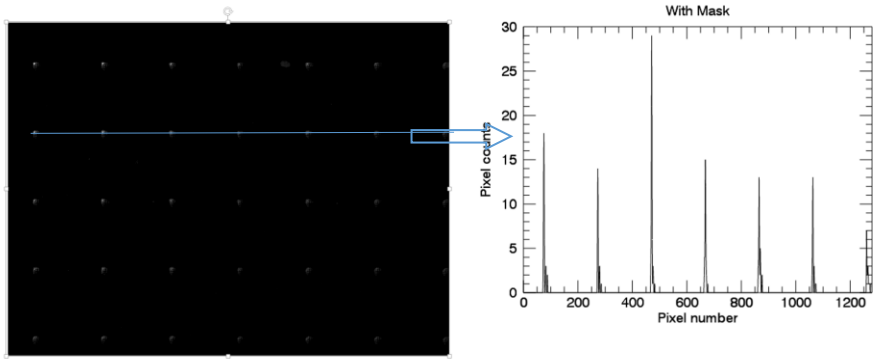

(c)

Figure 5. Patterns on the focal plane of lenslet array, which is also the back surface of the lenslet array. (a) The pattern for the bare lenslet array without pinhole mask. (b) The pattern for the lenslet array with pinhole mask at the center of the lenslet array. (c) The pattern for the lenslet array with pinhole mask, but off the center of the array.

From the initial test, we can make the following five points:

1. The lenslet array is made to the specification with the focal plane right on the back of the lenslet array surface.
2. The PSFs in the lenslet focal plane are diffraction limited. The diffraction limited pattern for square aperture is observed.

3. The intensity of the spots around the center of the lenslet array is about same with and without mask for the collimated light perpendicular to the lenslet array. This indicates that the pinhole mask is well aligned.
4. The diffraction from lenslet edge is removed by the pinhole mask, which reduces the contamination among the spectra.
5. The last one, also the unique feature of this innovative mask, is its capability to further suppress the speckles and increase the contrast. When the FOV of the CCD camera moves out of the center, the spots are getting dimmer and dimmer. The residual light from the star has a relative flat wavefront at the lenslet array. Therefore, the speckles at exoplanet FOV will be suppressed.

5. OPTICAL DESIGN

5.1 Optical Design

PISCES optics includes the following three main paortions: a relay optics, a key IFS element – lenslet array, and a prism spectrometer. The function of relay is to adjust the plate scale to match the required FOV to the designed lenslet size. The function of the lenslet array is to squeeze the light on each lenslet to a tiny spot to provide space for dispersing the spectra. From spatial resolution point of view, each lenslet is equivalent to one pixel in the image plane. The spectrometer is the same as normal prism spectrometers with a collimator, an imager, and a compound prism assembly. Only difference of this spectrometer is that it needs to deal with the multiple pupils created by each lenslet. It creates some challenges, but very manageable.

Figure 6 shows the layout of the PISCES optics. Based on the top level requirement and calculated lenslet size, the relay optics needs to provide a beam with f/# = 870. This means the relay needs to provide a large magnification (~10x). If two off-axis parabolic mirrors are used, the total track length will be very long. In order to make is more compact, an off-axis Ritchey–Chrétien telescope is selected. The big advantage of Ritchey–Chrétien type of relay has a very non-telecentric output. This is perfect for further suppressing the speckles using the combination of lenslet array and pinhole mask discussed in Section 4. In order to fit to the space designated to PISCES, a pick-off mirror and two fold mirrors are added.

Lenslet array design has been discussed in detail in section 4.

Spectrometer uses a common design. Because the magnification is unit, both collimator and imager have a same effective focal length. The beam is f/8 in both object plane and image plane. The multiple pupils make it impossible for the collimator and imager being identical, and the beam after the collimator is not aberration free. However, all these are not difficult to handle.

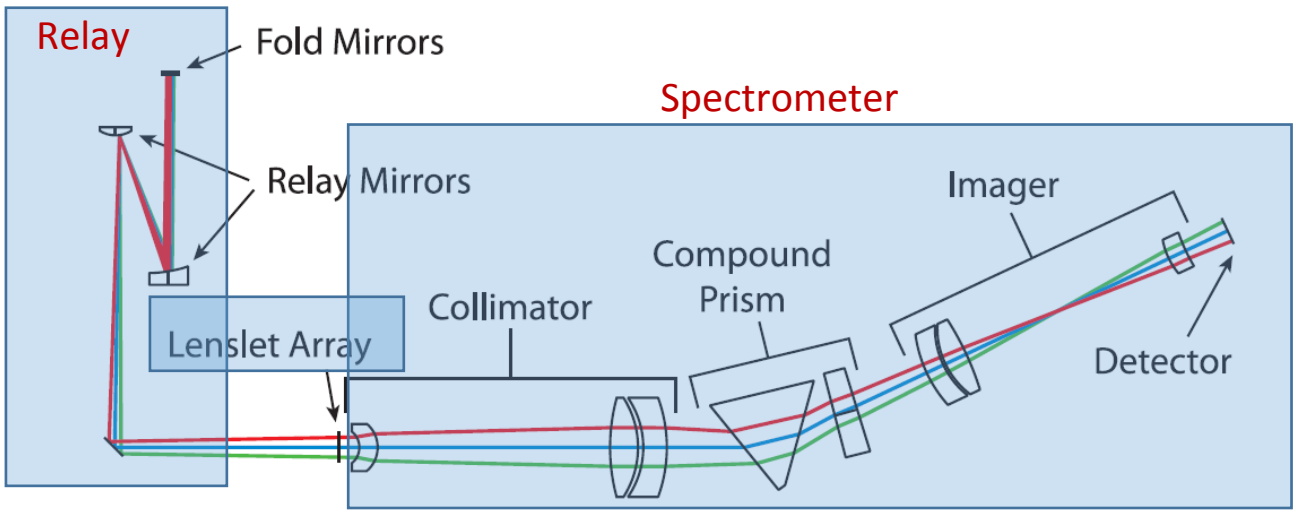

Figure 6. PISCES optics layout. It includes 3 portions: relay optics, spectrometer, and key IFS element – lenslet array.

5.2 Compound Prism Design and Trade-off

The two popular ways to create spectral dispersion are grating and prism. Since we have selected the lenslet array for PISCES, the grating is no longer a choice. Even though the spectral bandpass filter is used, the unwanted diffraction orders still contaminate spectrum. Especially, the required crosstalk for exo-planet application is much tighter than most other applications. So prism is selected as IFS dispersion element.

After the trade-off study, the final prism design uses a compound prism assembly with non-zero deviation. Even though zero-deviation provides some advantage for alignment and calibration, but the dispersion is extremely non-uniform. In comparison, non-zero deviation provides a much more uniform dispersion. On the other hand, single prism and compound prism are also compared. The compound prism with a prism and a compensator can provide near constant spectral resolution in the full wavelength range from 600nm to 970nm. Figure 7 shows the spectral resolution versus wavelength for a number of different study cases and the final PISCES spectral resolution.

To meet the requirement of spectral resolution of R=70, the apex angle of fused silica prism is designed at 54.65°, and that of ZnS compensator 3°. The wedges of the prism and the compensator are in opposite directions. The deviation angle for the central wavelength (740nm) is 25.13°.

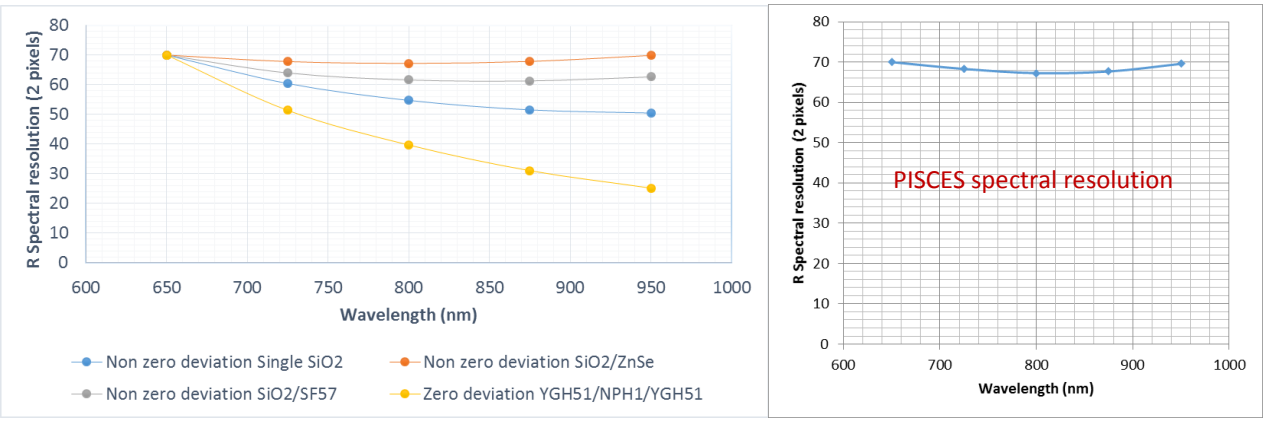

Figure 7. Spectral resolution versus wavelength. The plot on the left shows the trade-off for different study cases. The zero deviation prism has the most non-uniform resolution. Within the non-zero deviation cases, the single prism has the most non-uniform resolution. For multiple prism case, the uniformity depends on the material selection for the prism and compensator. The plot on the right is the final PISCES spectral resolution. The prism material is fused silica and the compensator is ZnS.

5.3 IFS Performance

The performance of the relay optics is diffraction limited. Because of the f/870 slow beam, the $f \cdot \lambda / D$ at 600nm is 522µm, that covers 3 lenslet as required. The spectrometer is not diffraction limited for the full FOV, but very close and meet the requirement that the RMS spot size from the design residual is less than one pixel size, which is 13 µm. With the fabrication and alignment tolerances added, the RMS spot size grows to 16 µm. Figures 8 and 9 show as-designed spatial and spectral performance.

The 2nd band is used to demonstrate the designed IFS meet the spectral resolution. For the 2nd band, the central wavelength $\lambda c = 770$nm. $\Delta\lambda = \lambda c / R = 770 / 70 = 11$nm. In the design, this 11nm has to be separated by 2 detector pixels to make sure they are resolvable. The right plot in figure 9 show that the 11nm is 26 µm apart, which is 2 pixels for the 13 µm pixel.

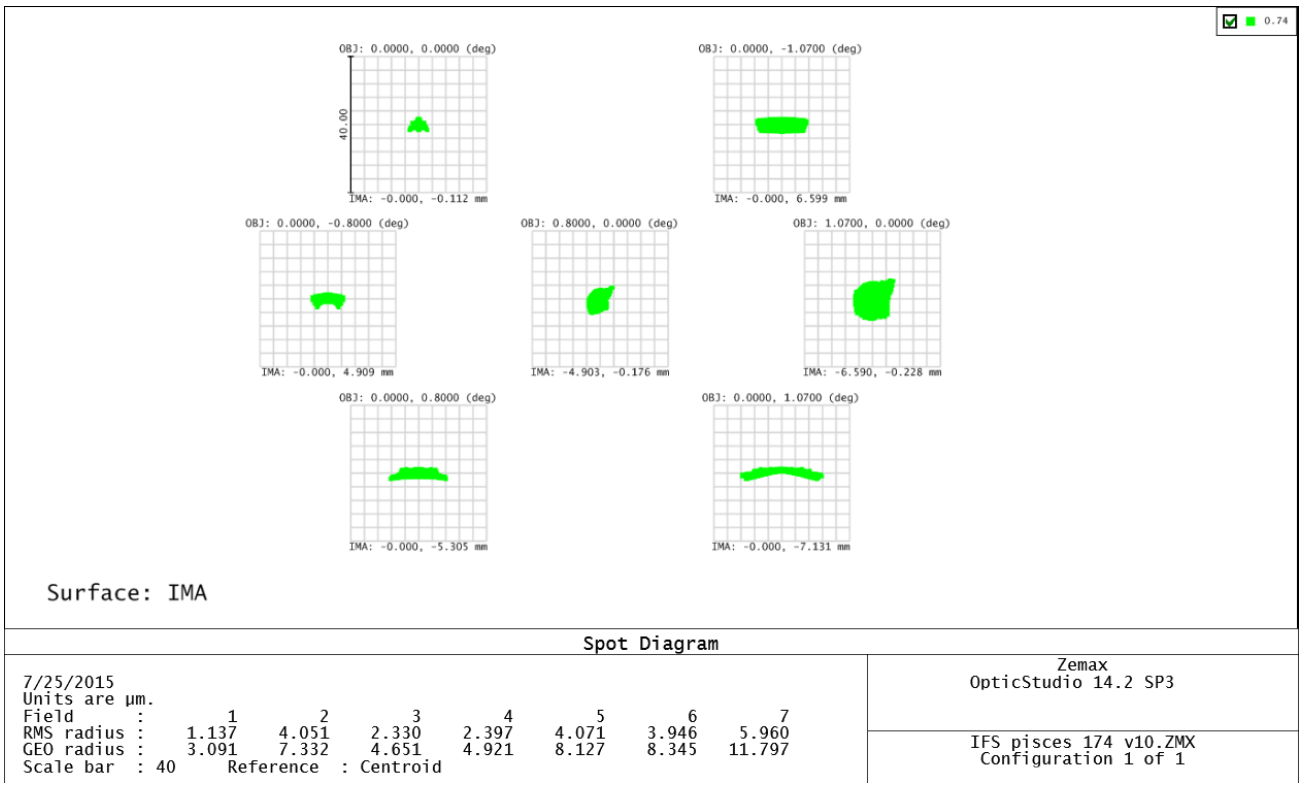

Figure 8. Spot diagram at the IFS detector for different fields at λ=740nm. Spot diagram is one of the ways to measure spatial resolution.

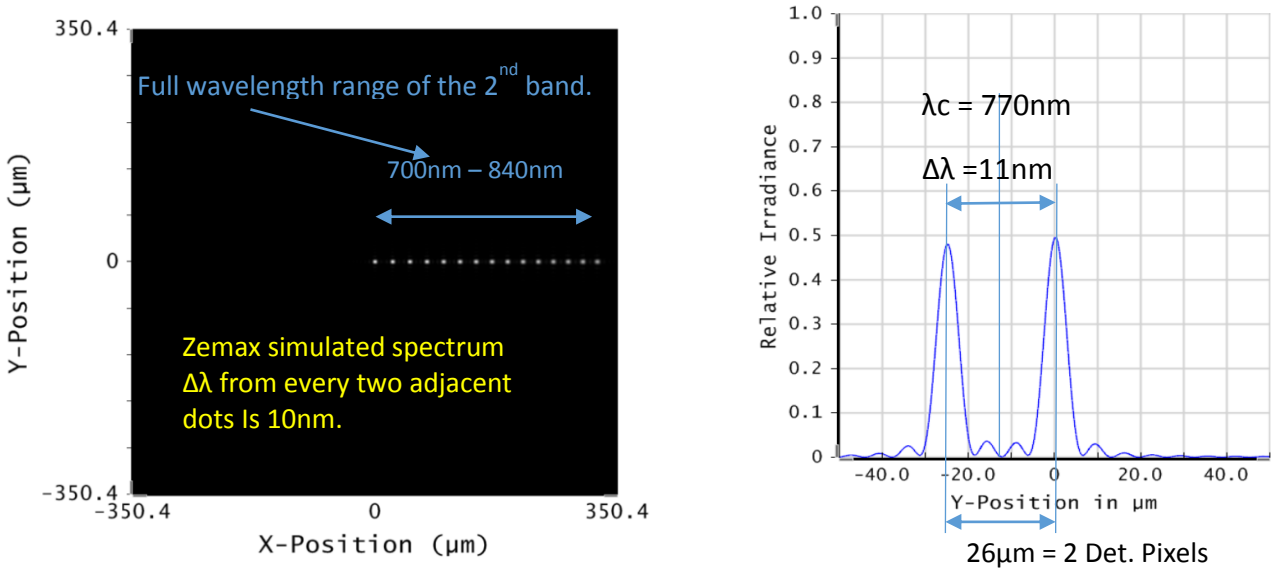

Figure 9. On the left is the Zemax simulated spectrum of the 2nd band from 700nm – 840nm. The plot on the right is lso generated by Zemax. Both are showing that the two adjacent wavelengths of R=70 is well separated.

5.4 Refractive Spectrometer Design Versus Reflective

A trade-off has been performed between refractive and reflective spectrometer for the coronagraph. Figure 10 (a) is the current PISCES design, and figure 10 (b) is a reflective design. The reflective design uses the crossed configuration that discreibed by Huan Tran, etc[8]. This design allows us to simplify collimator and imager from Three-Mirror Anastigmat (TMA) to a more compact two mirror configuration. Even so, the volume of the reflective is still larger than the volume of refractive. A trade-off between refractive and reflective is listed in Table 4. Note: the trade-off is based on the defined wavelength range from 600nm to 970nm. In this wavelength range most of the optical glasses have a very low absorption and dispersion is relatively easy to control. For UV or long wave infrared ranges, reflective system has to be used.

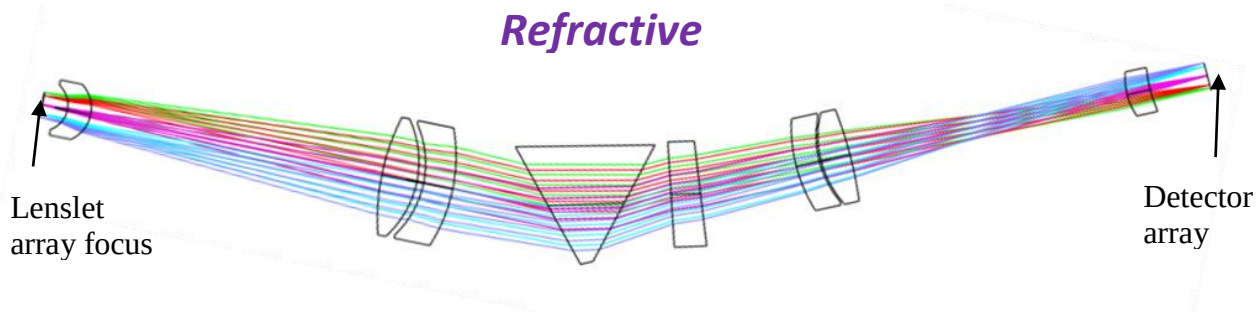

Figure 10 (a). PISCES refractive spectrometer design.

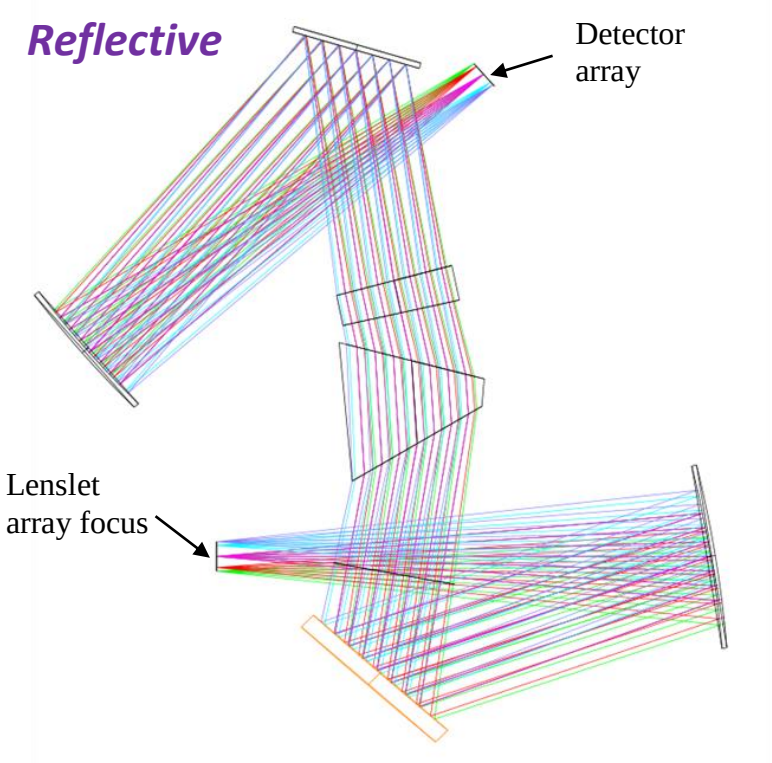

Figure 10 (b). A reflective design using the same IFS specification with the object from the same lenslet array.

Table 4. Refractive and reflective IFS trade-off.

		Pro	Con
Performance	Spot size	Refractive	Reflective
	Distortion	Reflective	Refractive
	X/Y aspect ratio	Refractive	Reflective
	Throughput	Reflective	Refractive
Volume		Refractive	Reflective
Fabrication		Refractive	Reflective
Alignment		Refractive	Reflective
Cost		Refractive	Reflective

Different people may end up with different conclusion based on their assumptions. Therefore, it is necessary to explain how we came up with the trade-off in Table 4. From performance point of view, refractive and reflective are pretty much even. Refractive is better for its image quality and provides a near 1:1 aspect ratio for X and Y in the image plane. For reflective, the throughput is slightly higher and the geometric distortion is also a little better. Volume wise, refractive is certainly better. Even a compact cross configuration optical design is used, the total area needed for reflective is 350mm x 350mm = 0.1225 m^2, and refractive under the same specification is 610mm x 120mm = 0.0732 m^2. The thickness of the reflective is also more than that of refractive. So the total volume between reflective and refractive is ~2:1. Fabrication wise, all refractive surfaces are standard spherical surfaces. The procedure to fabricate and align them are very mature. Even small optics shops have many test plates accumulated from so many years. With the additional help from interferometer, high quality lenses can be made cost efficiently. As for reflective, off-axis aspheric mirrors are needed, no matter it is crossed configuration or TMA. Undoubtedly, the technology development has improved the fabrication of aspheric surfaces dramatically, especially computer controlled diamond turning[9] and magnetorheological finishing[10]. However, CGH or null lens is still needed for testing each surface, except parabolic and limited conic surfaces. The metrology of aligning the aspheric surfaces are much more difficult. On the other hand, the air-bearing + indicator system that many optical companies have can easily align a lens with the tolerance less than 10 μm. However, a great effort is needed to align an aspheric surface to that accuracy with the high precision metrology tools, such as, high precision laser tracker or CMM, and high precision theodolites, etc. GSFC had built an IFS breadboard that is reflective. The element test, metrology and breadboard alignment is definitely not trivial. The difficult processes drive the cost up for reflective system. It is probably why the commercial cameras, even cell phone camera, are still refractive up to date.

6. OPTICAL ALIGNMENT

PISCES alignment includes two parts: One part is the alignment between JPL HCIT and GSFC PISCES. This alignment is to use two fold mirrors to realize. The pair of the fold mirrors acts like a periscope to raise the beam height from HCIT to defined height for PISCES. The tip and tilt of the two mirrors provide enough degrees of freedom to fine tuning the beam position and angle that goes into the relay optics. The other part is the PISCES internal alignment. This paper only addresses the alignment concept, not the detailed procedure.

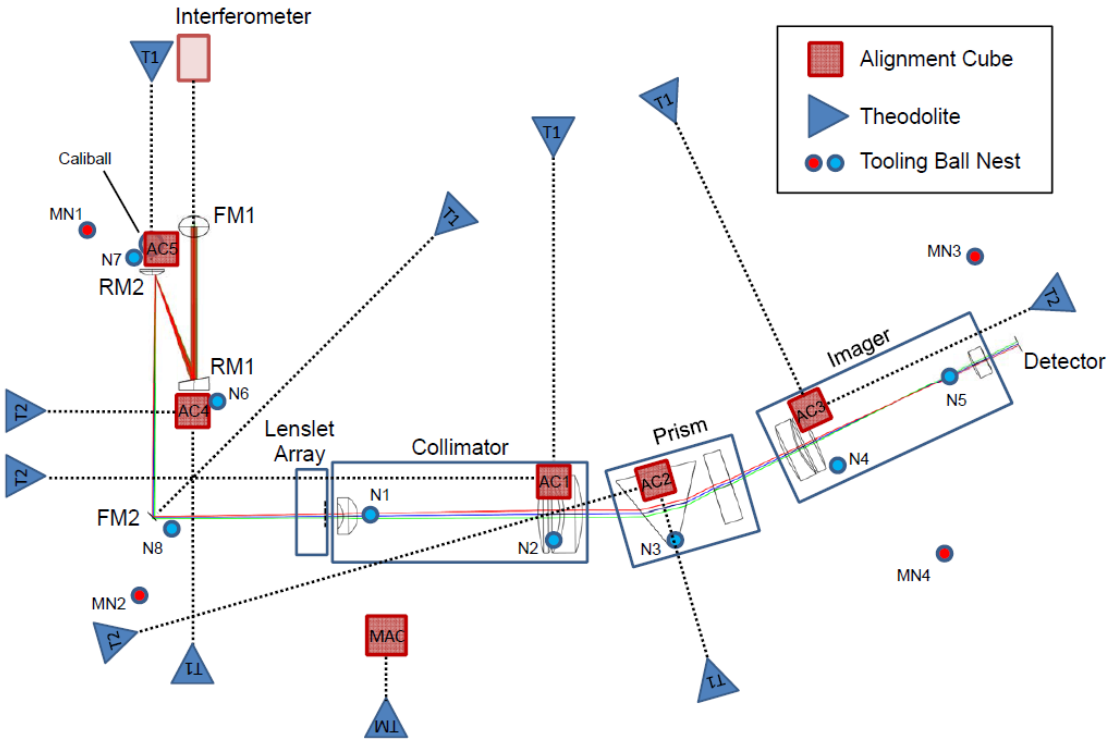

Figure 11. PISCES internal alignment plan schematic.

Figure 11 demonstrates our alignment concept based on the metrology and references on each element or sub-assembly. Note: to define a rigid body position in a global coordinate, it needs at least two directions (reference cube) and 1 position (Toolballl nest, target, to provide X, Y, and Z coordinate) or one direction and 2 positions. The following is the alignment summary:

1. Attach at least one alignment cube and one tooling ball nest to each element and sub-assembly.
2. Use theodolites, alignment telescopes, and Coordinate Measuring Machine (CMM) performing metrology of each element and sub-assembly to obtain the relationship between the element/sub-assembly and alignment references (cubes and nests).
3. Setup a Zemax alignment model to include the alignment references on all elements and subassemblies. To derive a table with all reference positions in a defined alignment coordinate.
4. Set master reference cube and nests to PISCES breadboard. These references have two functions: (a) if the theodolite or laser tracker has lost its reference due to accident, it can be recovered using these cubes and targets on the breadboard. (b) It will be very useful when the PISCES is to be aligned to HCIT at JPL.
5. To used metrology tools (theodolites and CMM) aligning each element and sub-assembly to the pre-determined positions.
6. The interferometer will be used to verify the wavefront at some key intermedia stages, fine tuning will be performed if necessary.
7. Record the angle and position of each cube and target relative to the master cube and nests. These will be re-checked when PISCES is shipped to JPL.

7. MECHANICAL DESIGN AND HARDWARE

PISCES mechanical design is relatively straight forward. A 5-axis stage is under every element and sub-assembly except the fold mirrors where only tip/tilt and the translation along the mirror normal is provided. All stages, as well as fold mirror mounts, are Commercial Off-The-Shelf (COTS) items. Figure 12 shows PISCES bench populated with mechanical mounts and stages. The optical designed is overlaid to show the optical element positions relative to the mechanical layout.

So far, the optics bench has been fabricated. All COTS items have arrived. The two critical optical elements in relay, an off-axis parabola and a hyperbola, have been fabricated and tested. The wavefront error of both mirrors meets the specification. The metrology of the references relative to mirrors optical axes and surface vertices has been completed. They are ready to be aligned to the bench.

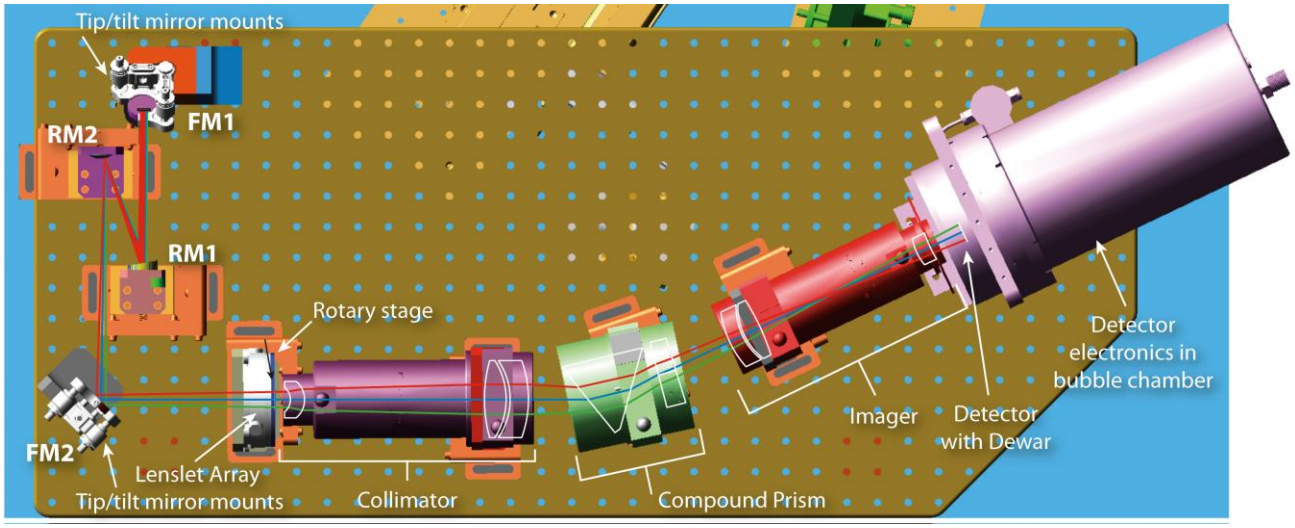

Figure 22. Top view of PISCES mechanical layout.

The lenslet array has been received and tested. The details have been discussed in Section 4.

The three assemblies in the spectrometer: collimator, compound prism, and imager, have been contracted out to an outside vendor. The expected delivery date is in late August to early September. The contract covers entire sub-assembly, including optical elements, surface anti-reflection coatings, mechanical mounts and barrels, and sub-assembly final test. After they are delivered, they will be assembled to the bench and aligned to relay and lenslet array. Final tests and calibration will be performed.

8. PISCES TEST AND CALIBRATION PLAN

PISCES final tests include spatial and spectral resolution tests, as well as spectral calibration. The spatial resolution tests include PSF test versus field and wavelength. The encircled energy will be used as the criterion. The spectral resolution will be judged by using two wavelengths with the separation of R = 70, which will be performed in all 3 wavelength bands and at different field positions. The spectral cross-talk will be measured. The challenge of this test is the pinhole mask on the back of the lenslet array surface. Our pinhole mask pattern follows the ray trace, that means the relay optics and a HCIT equivalent simulator is needed to generate the beam having the rays that hit the center of each lenslet with the same angle as the beam from HCIT. So our simulator is consist of the last three OAPs of HCIT. The three OAPs provide enough flexibility to add coronagraph masks at the intermediate focus or Lyot stop if necessary. The simulator layout is shown in Figure 13.

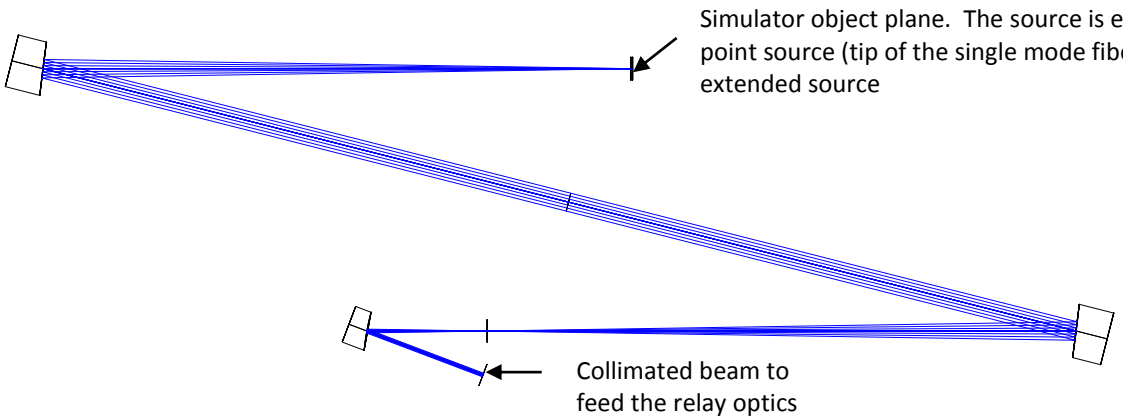

Figure 33. HCIT simulator for PISCES.

The light source for the test and calibration is to be a super-continuum source from NKT that provides a continuous wavelength coverage from 400nm to 2500nm. A module "VARIA" is a tunable filter that fully covers PISCES wavelength range from 600nm to 970nm. The wavelength bandwidth is adjustable from 4nm to 100nm. For spatial and spectral resolution tests, the tip of the single mode fiber will be used as a point source. The tip of the fiber moves in the object plane of the simulator to provide the field positions to be tested. Because PISCES IFS uses non-zero deviation prism assembly, the spatial resolution test and spectral test are very similar. Only difference is that the spatial resolution need only one wavelength, and the spectral resolution needs two wavelengths with the separated satisfying R = 70. The PSF on detector will be recorded and analyzed to evaluate if the specification is met. During the spectral test, the images of full bandwidth for the 3 bands (600nm -720nm, 700nm – 840nm, and 810nm – 970nm) will also be taken to verify if the spectra have the correct length and parallel to the rows of the detector array around the central field.

The source for calibration is the same super-continuum source but being used a little differently. For calibration, we basically need to have the monochromatic images of the full FOV to calibrate out spatial and spectral distortions. So the light at the simulator object plane has to be an extended source to cover the full FOV. As mentioned before, the simple collimated light before the lenslet array will not pass all pinholes on the mask because the mask is designed for non-telecentric system. So the plan is to move the fiber back from the simulator object plan, and to insert one or two diffractive diffusors between the tip of the fiber and the object plane to make sure the light distribution at the object plane is uniform enough with the f/# to match the simulators. Three to five wavelengths will be used for each wavelength band. The image from each wavelength (76 x 76 PSFs) will be recorded. These images include all spatial and spectral information: geometric and spectral distortion, dispersion versus wavelength, throughput, etc. The images from each wavelength band will be reformatted to what the calibration software requests.

The on-orbit calibration plan will be developed with incorporation of coronagraph instrument team. If the coronagraph masks is always fixed for the entire mission, the stars are not the valid targets for on-orbit calibration, because the most of the light is blocked by masks.

9. CONCLUSION

In this section, we'll summarize the PISCES status and discuss the path forward. The PISCES design and analysis, including optical, mechanical, and thermal, has been completed. All hardware either has received or in procurement stage with an estimated delivery date. The received optical elements have been tested and meet specification. All mechanical parts have been received, except three spectrometer subassemblies that are contracted out. The HCIT simulator and relay optics is being aligned. The lenslet array with pinhole mask has been tested and the result agrees with what we expected.

The path forward is to complete the simulator and relay optical alignment and to get ready for aligning and assembling the lenslet array and the spectrometer when the sub-assemblies are delivered. Meanwhile the detailed procedures will be

generated based on the final PISCES test and calibration plan. The equipment and setup required for the final test and calibration will be prepared. We plan to deliver the PISCES to JPL in February of 2016 and integrate it to HCIT testbed.

REFERENCES

[1] "Exoplanet" from Wikipedia, https://en.wikipedia.org/wiki/Exoplanet

[2] "Methods of detecting exoplanets" from Wikipedia, https://en.wikipedia.org/wiki/Methods_of_detecting_exoplanets

[3] "WFIRST-AFTA Science Definition Team Final Report", http://wfirst.gsfc.nasa.gov/science/sdt_public/WFIRST-AFTA_SDT_Report_Briefing_to_Hertz_150219_Final_RevA.pdf

[4] John Trauger and AFTA coronagraph design team, "High contrast Image Testbed (HCIT) at JPL," http://home.strw.leidenuniv.nl/~kenworthy/_media/nospeckles:leiden_hcit_141008.pdf

[5] "Integral Field Spectroscopy Wiki", http://ifs.wikidot.com/what-is-ifs

[6] Qian Gong and Michael McElwain, "A Novel Lenslet Coupled Pinhole Mask to Suppress Starlight for High Contrast Imaging," NASA New Technology Report (NTR) GSC-16578-1 (2012)

[7] Jorge Llop Sayson, Nargess Memarsadeghi, Michael W. McElwain, Qian Gong, Marshall Perrin, Timothy Brandt, Bryan Grammer, Bradford Greeley, George Hilton, Catherine Marx, "PISCES: high contrast integral field spectrograph simulations and data reduction pipeline," submitted Proc. SPIE 9605 (2015)

[8] Huan Tran, Adrian Lee, Shaul Hanany, Michael Milligan, and Tom Renbarger, "Comparison of the crossed and the Gregorian Mizuguchi–Dragone for wide-field millimeter-wave astronomy," Applied Optics, 47(2), 103-109 (2008)

[9] Mark Craig Cerchman, "Specifications and manufacturing considerations of diamond machined optical components," Proc. SPIE 0607, 36-45 (1986)

[10] Donald Golini, William I. Kordonski, Paul Dumas, Stephen J. Hogan, "Magnetorheological finishing (MRF) in commetial precision optics manufacturing," Proc. SPIE 3782, 80-91 (1999)